APL Photonics

RESEARCH ARTICLE | FEBRUARY 14 2024

Cluster synchronization in a semiconductor laser

Dmitry Kazakov ; Nikola Opačak; Florian Pilat ; Yongrui Wang ; Alexey Belyanin ; Benedikt Schwarz ; Federico Capasso

APL Photonics 9, 026104 (2024)
https://doi.org/10.1063/5.0187078

Cluster synchronization in a semiconductor laser

Cite as: APL Photon. 9, 026104 (2024); doi: 10.1063/5.0187078
Submitted: 10 November 2023 • Accepted: 23 January 2024 •
Published Online: 14 February 2024

Dmitry Kazakov,[1,2,a] Nikola Opačak,[1,2] Florian Pilat,[2] Yongrui Wang,[3] Alexey Belyanin,[3] Benedikt Schwarz,[1,2,b] and Federico Capasso[1,c]

AFFILIATIONS

[1] Harvard John A. Paulson School of Engineering and Applied Sciences, Harvard University, Cambridge, Massachusetts 02138, USA
[2] Institute of Solid State Electronics, TU Wien, 1040 Vienna, Austria
[3] Department of Physics and Astronomy, Texas A & M University, College Station, Texas 77843, USA

[a] **Author to whom correspondence should be addressed:** kazakov@seas.harvard.edu
[b] benedikt.schwarz@tuwien.ac.at
[c] capasso@seas.harvard.edu

ABSTRACT

Cluster synchronization is a general phenomenon in a network of non-locally coupled oscillators. Here, we show that cluster synchronization occurs in semiconductor lasers, where the beat notes between the pairs of adjacent longitudinal modes of the laser cavity constitute a collection of coupled phase oscillators. Non-local coupling arises from the standing-wave nature of the cavity with finite mirror reflectivities, which we can actively control. Varying the coupling, we can bring the laser into a state of cluster synchronization where the two beat note families oscillate at two distinct collective frequencies. Using a coherent beat note detection technique, we show that the beat notes within the two families are synchronized in the opposite configurations—in-phase and antiphase.

Several animals sleep with half of their brain awake.[1] In this unihemispheric sleep phase, the neurons in the two halves of the brain show drastically different electrical activity.[2] Such a state of desynchronization is a general phenomenon in a collection of coupled identical oscillators, where the coupling strength between all possible oscillator pairs is not uniform, whereas the function describing the coupling to the neighbors—the so-called coupling kernel—is the same for each given oscillator. Contrary to the case of global coupling, where equal interaction strengths between all oscillator pairs lead to the global synchronization of the entire population, in such a non-locally coupled system, the oscillators may synchronize in clusters. An ultimate example of cluster synchronization is a chimera state.[3] A chimera state is characterized by the presence of two sub-populations within the coupled oscillator array, whereby one subpopulation is perfectly in synchrony and oscillates as a whole, while the other is desynchronized. Cluster synchronization and chimera states are encountered in mechanical,[4,5] chemical,[6] and biological systems.[7] Understanding of the universal dynamics and the causes of the formation of such states is essential for the mitigation of catastrophic outages in power grid networks,[8] the prevention of partial seizures in brain,[9] and the treatment of cardiac arrests caused by ventricular fibrillation due to the desynchronization of the pacemaker cells in the heart muscle.[10]

In photonic systems, chimeras, or cluster states, may exist in spaces spanned by the coordinates, associated with various degrees of freedom of the electromagnetic wave. The most straightforward example is that of an array of coupled waveguide resonators, where the clustering manifests itself in the space-dependent intensity values at the output plane of the array along the lateral spatial dimension.[11] In passive nonlinear optical resonators, on the other hand, individual coupled oscillators, constituted by the values of the optical field intensity along the cavity coordinate, have been shown to produce regions of random intensity oscillations bounded in time by regions of constant intensity.[12] In active laser cavities, where multiple longitudinal modes can be above the threshold simultaneously, giving rise to an optical frequency comb, clustering can manifest itself in a wavelength-dependent linewidth of the individual comb teeth.[13] There, the oscillators are arranged along a synthetic frequency (or wavelength) dimension in the reciprocal space.[14]

Here, we show that in a semiconductor laser, the non-locally coupled oscillators constituted by the radio frequency intermode

beatings, and arranged along the optical frequency dimension, may synchronize in clusters. To conceptually introduce the phenomenon of cluster synchronization and its key properties, we first consider the Kuramoto model of a family of coupled phase oscillators [Fig. 1(a)].[15] The Kuramoto model has widely been applied to study systems featuring a spontaneous onset of synchrony, e.g., in ensembles of fireflies,[16] neuronal cell networks,[17] human crowds,[18] and mechanical oscillators.[5] Later, we consider a full laser model, which can also be regarded as a coupled oscillator model but departs substantially from the Kuramoto model. Nevertheless, the key qualitative evidence of cluster synchronization pertains to both systems. In the Kuramoto model, the dynamics of a collection of N phase oscillators (i.e., all oscillators swinging with the same amplitude) is traced by the temporal evolution of the phases θ_i of these oscillators,

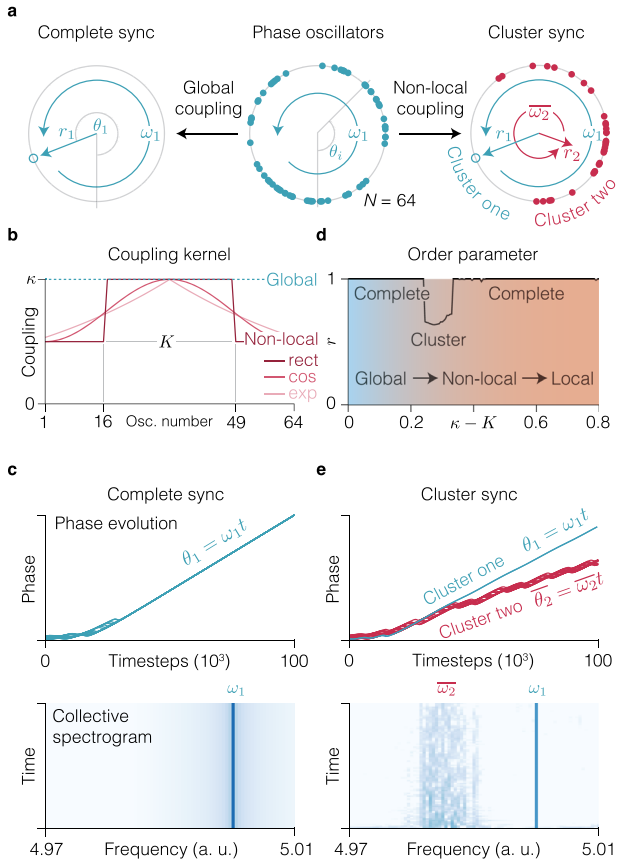

FIG. 1. (a) Initially randomly distributed phases of $N = 64$ oscillators (filled turquoise dots) with identical natural frequencies ω_1 attain the state of complete synchronization in case of global coupling (all N oscillator phases become identical as represented by the unfilled turquoise dots), or split into clusters under non-local coupling (the completely synchronized cluster composed of $N/2$ oscillators is represented by the unfilled turquoise dots). (b) Various functional shapes of the coupling kernel that defines the coupling strength of each possible oscillator pair. (c) (Top) Simulated phase trajectories of $N = 64$ oscillators for $\kappa - K = 0.1$. (Bottom) Spectrogram of the time-evolving collective oscillation. (d) Kuramoto order parameter r, for a range of coupling disparities. (e) Phase trajectories of the $N = 64$ oscillators for $\kappa - K = 0.25$ and the collective spectrogram of the cluster state.

$$\dot{\theta}_i = \omega_1 - \sum_{j=1}^{N} f(|j-i|)\sin(\theta_j - \theta_i + \phi), \tag{1}$$

where $\dot{\theta}_i$ is the time derivative of the phase of the ith oscillator—or its instantaneous frequency, ω_1 is its natural angular frequency, identical for all oscillators, ϕ is a collective phase delay, and $f(|j-i|)$ is the coupling kernel that defines the distance-dependent coupling strength between the jth and the ith oscillators. In the simulations of the Kuramoto model, we assume a periodic boundary condition and a symmetric coupling kernel—oscillators are arranged on a ring such that oscillator $i = N$ is coupled equally strongly to oscillators $j = N - 1$ and $j = 1$. Under the condition of global coupling $f(|j-i|) = \kappa$, where $\kappa \leq 1$ is a scalar [Fig. 1(b)], complete synchronization occurs, signified by the phase locking of the initially randomly distributed oscillator phases [Fig. 1(a)]. The temporal evolution of the individual oscillator phase angles θ_i, once in synchrony after an initial transient, is linear in time with a slope equal to the collective oscillation frequency: $\theta_1 = \omega_1 t$ [Fig. 1(c)]. One way to visualize the state of synchronization is to construct the collective spectrogram of the oscillators by summing the instantaneous angles of all oscillators $E(t) = \sum_j^N \cos(\theta_j(t))$ and taking a short-time Fourier transform of $E(t)$. In case of complete synchronization, such a spectrogram features a single narrow peak at the collective frequency ω_1 [Fig. 1(c)].

Cluster synchronization, on the other hand, can occur in a non-locally coupled system. Non-local coupling can be introduced in Eq. (1) using a boxcar kernel [Fig. 1(b)],

$$f(|j-i|) = \begin{cases} \kappa & \text{if } |j-i| \leq N/2, \\ K & \text{if } |j-i| > N/2. \end{cases}$$

The functional form of $f(|j-i|)$ can vary: other types of the coupling kernel, such as cosine $f(|j-i|) = K + (\kappa - K)\cos(|j-i|)$ or exponential $f(|j-i|) = K + (\kappa - K)\exp(|j-i|)$, lead to the same synchronization dynamics [Fig. 1(b)].[3] The key parameter that defines the type of the synchronization state is the coupling disparity $\kappa - K$. For $\kappa - K$ small, when the oscillators can still be seen as globally coupled, as well as for $\kappa - K$ large, when the system is effectively locally coupled, it attains the state of complete synchronization, which is characterized by a high degree of mutual phase coherence between the oscillators. The degree of phase coherence in the steady state can be quantified with the Kuramoto order parameter,

$$r = \frac{1}{N}\left|\sum_{j=1}^{N} \exp(i\theta_j)\right|. \tag{2}$$

Complete in-phase synchronization is signified with $r = 1$ [Fig. 1(d)]. For an intermediate range of values of $\kappa - K$, the system is coupled non-locally and splits into two clusters, resulting in the reduction of the order parameter: $r < 1$ [Fig. 1(d)]. The collective frequencies of the oscillator clusters are not the same, as seen from the different slopes of phase evolution of the oscillators [Fig. 1(e)]. Moreover, while the oscillators in the first cluster are completely synchronized, after the initial transient, the oscillators in the second cluster, despite moving at a well-defined mean frequency, have a lower mutual coherence, i.e., they are not phase-locked to each other [Fig. 1(e)]. The spectrogram in the cluster synchronization state features two distinct tones—one narrow centered at the

mean frequency of the fully synchronized cluster and the other broad centered at the frequency of the partially synchronized cluster [Fig. 1(e)]. Such a state of a system where the fully coherent cluster and an incoherent cluster coexist in a population of identical oscillators is also known as a chimera state.[3] However, the fact that the collective frequencies are distinct and well-separated is not obvious and is an important corollary of this simulation that is not given its due in the literature.[15,19] While, intuitively, the collective frequency of the first, coherent, cluster ω_1 coincides with the natural frequency of the oscillators, the frequencies of the oscillators in the incoherent cluster are not spread around the natural frequency but rather around the mean value of $\overline{\omega_2} \neq \omega_1$. This separation of the collective frequencies will be one of the defining features of cluster synchronization in a semiconductor laser.[13] In a laser cavity where multiple longitudinal modes can simultaneously be above the threshold, the oscillators are the beat notes between the pairs of neighboring cavity resonances [Fig. 2(a)].[20] One mode of their synchronization is the so-called splayed phase (or antiphase) state, when the phases between the intermode beat notes across the laser spectrum cover the range from 0 to 2π, such that for each intermode beat note, there is another one that is π out of phase with it. Such a state leads to frequency-modulated (FM) comb emission in free-running semiconductor laser of various types: quantum dot,[21] quantum dash,[22,23] quantum well,[24,25] interband cascade,[26] and quantum cascade lasers (QCLs).[27–29] On the contrary, in actively and passively mode-locked semiconductor lasers, all intermode beat notes can have the same phase, and the laser generates a pulsed amplitude-modulated (AM) frequency comb.[21]

Here, we show that both synchronization states—FM and AM—occur simultaneously in a Fabry–Pérot quantum cascade laser (QCL). Such a state is a cluster synchronization state and is attained in the regime when the intermode beat notes are coupled non-locally within the standing-wave laser cavity. A qualitative analogy with the oscillators in the Kuramoto model is as follows: In a QCL, once multiple longitudinal cavity modes are simultaneously above the lasing threshold, the pairwise beating between each pair of neighboring cavity modes will create a temporal modulation of the population inversion at frequencies close to the cavity round trip frequency—several tens of GHz for a typical cavity length of few millimeters [Fig. 2(a)]. Each of these intermode beat notes can be seen as an individual microwave oscillator, and as a whole, they form a collection of oscillators that are coupled by the very same laser gain medium that generates them (see Sec. I of the supplementary material).[30] Due to the frequency dependence of the effective refractive index (i.e., the cavity dispersion), the natural frequencies of these oscillators are not identical; however, they can synchronize via $\chi^{(3)}$ four-wave mixing nonlinear interactions inside the gain medium, which corresponds to the action of the forcing term $\sin(\theta_j - \theta_i)$ in Eq. (1).[31–33]

The coupling disparity between different beat note pairs arises as follows: In a standing-wave cavity, the coupling strength between

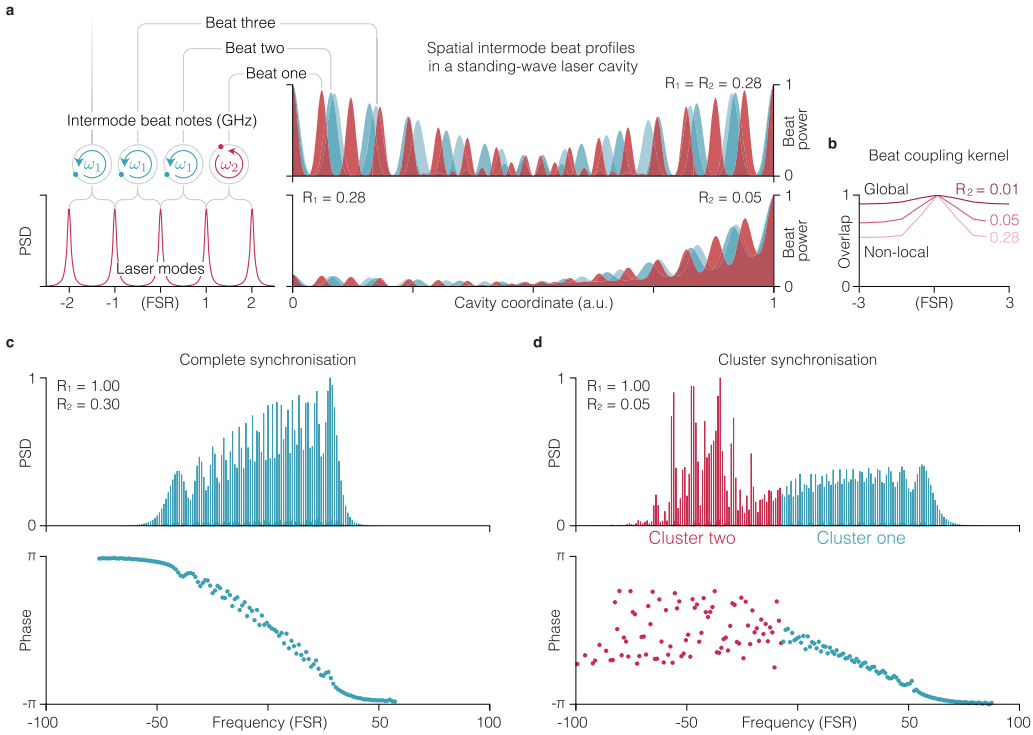

FIG. 2. (a) Spatial profiles of the intermode beat notes between the longitudinal laser modes inside the laser cavity. R_1 and R_2 are the end facet mirror reflectivities. (b) Coupling strength as a function of spectral separation, calculated as an overlap integral between the spatial profiles of the corresponding beat notes. Increasing R_2 results in a transition from global coupling ($R_2 = 0.01$) to non-local coupling ($R_2 = 0.28$). (c) Power spectral density (PSD) and beat note phase of the simulated laser in a steady state with $R_1 = 1$ and $R_2 = 0.3$. (d) PSD and beat note phase of the simulated laser in a steady state with $R_1 = 1$ and $R_2 = 0.05$.

two intermode beat notes is proportional to the overlap of their spatial profiles.[20,30] The analog of the coupling kernel can then be defined by computing the spatial overlap integral along the cavity axis for each pair of intermode beat notes [Fig. 2(a)]. This overlap is high for the beat notes generated by the neighboring mode pairs and is lower for the beat notes of more distant mode pairs. In this picture, the beat notes are the oscillators that are arranged along a synthetic optical frequency axis, and the coupling strength fades away the larger the distance is between the points on the frequency axis [Fig. 2(a)]. As a result, each intermode beat note is coupled stronger to its nearest neighbors than to the more distant ones, giving rise to an effectively non-local coupling kernel as in the Kuramoto model [Fig. 1(b)]. The coupling disparity can be tuned by changing the reflectivity of one of the end facet mirrors: a highly asymmetric cavity results in global mode coupling, whereas a symmetric cavity results in non-local coupling [Fig. 2(b)]. To elucidate the effect of the coupling disparity induced by the asymmetry of the cavity, we show the result of the spatiotemporal simulation of the Maxwell–Bloch model of QCLs for the cases of two different facet reflectivities. The model and the simulation tool are adapted from Ref. 34. In both simulated cases, the left facet reflectivity is $R_1 = 1$. For the right facet reflectivity $R_2 = 0.3$, the laser modes synchronize completely with a well-defined and constant splayed phase relationship among the intermode beatings [Fig. 2(c)]. In case of $R_2 = 0.05$, the laser spectrum splits into two clusters, whereby the beatings in the first cluster are synchronized in a splayed phase configuration, whereas the beatings in the second cluster are less coherent—they assume a uniform phase spread around a well-defined mean value. This state is not a transient one and persists for the entire duration of the simulation. Due to the coexistence of coherence and incoherence within the beat note family, this state of the laser indicates similarity to a chimera state [Fig. 2(d)].

We generate such cluster states experimentally in a Fabry–Pérot QCL with an active region based on the so-called bifunctional design,[35] grown on an InP substrate and processed as a buried heterostructure. The bifunctional design allows for active control of absorption within the gain region. To enable the tuning of the coupling kernel, we realize a mirror with adjustable reflectivity by splitting the top laser contact into a long gain section (3.3 mm) and a short mirror section (0.4 mm), which can be biased independently, inducing variable absorption at the cavity facet (see Sec. II of the supplementary material). At a low bias, absorption results in effective lower end facet reflectivity, and at a high bias, when the absorption is lower, the effective reflectivity increases. This variable mirror section enables active control of the coupling disparity. Furthermore, the short section allows for efficient microwave extraction and injection into the laser by bringing a ground-signal (GS) radio frequency probe in contact with it.[36]

By tuning the biases of the gain and the mirror sections, we can selectively bring the laser in one of the two possible synchronization states. In one of them—the antiphase synchronization state—the laser spectrum consists of a strong carrier with two sidebands [Fig. 3(a)], which are π out of phase (see Sec. II of the supplementary material on the details of the experimental phase retrieval). The RF spectrum of the laser output around the cavity repetition frequency shows one narrow (sub-kHz linewidth) and weak tone—the result of incomplete destructive interference of the two out of phase intermode beatings.

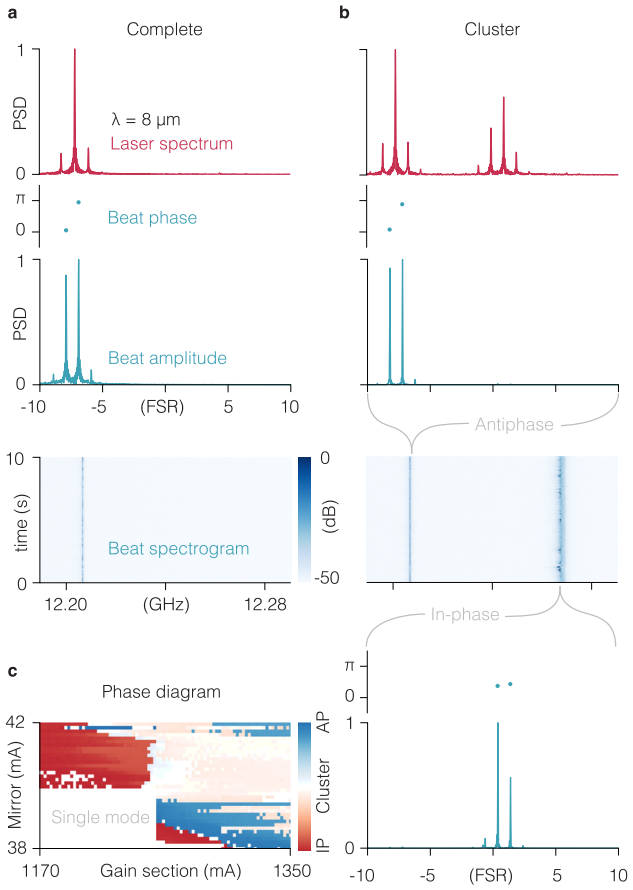

FIG. 3. (a) Power spectral density (PSD), intermode beat note phases, and intermode beat note intensities of the laser operating in an antiphase synchronization regime. FSR, free spectral range. The laser spectrum is centered at 1256.6 cm^{-1} (7.96 μm). (b) PSD, intermode beat note phases, and intermode beat note intensities for the laser in a cluster synchronization regime. (c) Phase diagram of the laser state as a function of two parameters—a long gain section DC bias current density and a short mirror section DC bias current density.

Increasing the bias on the short laser section, we can bring the laser to a cluster synchronization state. In this state, the laser spectrum consists of two mode families synchronized at two different collective frequencies [Fig. 3(b)]. Notably, the RF tone at 12.24 GHz is more broad than its lower frequency counterpart at 12.20 GHz, which signifies the reduced coherence of the collection oscillating at 12.24 GHz, in correspondence with simulations [Fig. 2(d)]. Power spectrum of the laser emission alone does not allow to ascribe each of the RF tones to a particular mode cluster. However, from parallel demodulation at these two collective frequencies (RF_1 and RF_2), we unambiguously show the correspondence between the two distinct mode clusters visible in the laser spectrum and the two RF beat notes visible in the spectrogram. In the red detuned cluster, the beat notes are synchronized in antiphase, and in the blue detuned cluster—in-phase [Fig. 3(b)]. Continuous sweeping of the two parameters—currents in the gain and the mirror laser sections—results in sharp transitions between the antiphase

and cluster states that are signified by the appearance and disappearance of the respective tones in the RF spectrum. The two bias controls span a two-dimensional phase space, in which the states of the laser live [Fig. 3(c)]. As in the case of the Kuramoto model, cluster synchronization occurs in the intermediate range of coupling disparities, controlled by the mirror section bias.

Cluster state is a remarkable manifestation of the generality of the synchronization phenomena. In laser systems, cluster synchronization should not be restricted to QCL gain media: it could potentially be attainable in any laser where multiple longitudinal modes can oscillate simultaneously. The recent observation of in-phase and antiphase synchronization modes in a quantum dot laser suggests that cluster state is another possible mode of operation of these lasers.[21] Furthermore, in solid-state laser cavities that support a large number of transverse modes where non-local coupling can be implemented with specially designed intracavity optical elements, synchronization and clustering can potentially occur among the spatially coherent structures in the beam cross section.[37] In semiconductor lasers, mode clusters are as well known to arise due to the presence of higher order dispersion in the laser cavities. In case of QCLs, such clustering, due to higher order dispersion, does not lead to the synchronization state of the type presented here. Instead, the modes in two clusters remain fully in synchrony throughout the spectral bandwidth.[38,39]

If viewed as a regime to avoid, the cluster state, seemingly inherent to Fabry–Pérot cavities, should not appear in traveling-wave ring cavities, where the spatial beat note profiles are uniform and the coupling is global. From this perspective, recently demonstrated ring QCL frequency combs could have a superior noise and stability performance.[40–44]

Description of experiments and theoretical model.

This project has received funding from the European Research Council (ERC) under the European Union's Horizon 2020 research and innovation program (Grant Agreement No. 853014).

AUTHOR DECLARATIONS

Conflict of Interest

The authors have no conflicts to disclose.

Author Contributions

Dmitry Kazakov: Conceptualization (equal); Data curation (equal); Formal analysis (equal); Writing – original draft (equal). **Nikola Opačak**: Conceptualization (equal). **Florian Pilat**: Data curation (equal); Formal analysis (equal). **Yongrui Wang**: Conceptualization (equal); Writing – original draft (equal). **Alexey Belyanin**: Conceptualization (equal); Writing – original draft (equal). **Benedikt Schwarz**: Supervision (equal); Writing – original draft (equal). **Federico Capasso**: Supervision (equal); Writing – original draft (equal).

DATA AVAILABILITY

The data that support the findings of this study are available from the corresponding author upon reasonable request.

REFERENCES

[1] C. Koch, "To sleep with half a brain," Sci. Am. Mind **27**, 22–25 (2016).
[2] L. M. Mukhametov, A. Y. Supin, and I. G. Polyakova, "Interhemispheric asymmetry of the electroencephalographic sleep patterns in dolphins," Brain Res. **134**, 581–584 (1977).
[3] D. M. Abrams and S. H. Strogatz, "Chimera states for coupled oscillators," Phys. Rev. Lett. **93**, 174102 (2004).
[4] M. Kapitaniak, K. Czolczynski, P. Perlikowski, A. Stefanski, and T. Kapitaniak, "Synchronous states of slowly rotating pendula," Phys. Rep. **541**, 1–44 (2014).
[5] E. A. Martens, S. Thutupalli, A. Fourrière, and O. Hallatschek, "Chimera states in mechanical oscillator networks," Proc. Natl. Acad. Sci. U. S. A. **110**, 10563–10567 (2013).
[6] M. R. Tinsley, S. Nkomo, and K. Showalter, "Chimera and phase-cluster states in populations of coupled chemical oscillators," Nat. Phys. **8**, 662–665 (2012).
[7] M. Lodi, F. Della Rossa, F. Sorrentino, and M. Storace, "Analyzing synchronized clusters in neuron networks," Sci. Rep. **10**, 16336 (2020).
[8] A. E. Motter, S. A. Myers, M. Anghel, and T. Nishikawa, "Spontaneous synchrony in power-grid networks," Nat. Phys. **9**, 191–197 (2013).
[9] F. De Vico Fallani, J. Richiardi, M. Chavez, and S. Achard, "Graph analysis of functional brain networks: Practical issues in translational neuroscience," Philos. Trans. R. Soc., B **369**, 20130521 (2014).
[10] J. M. Davidenko, A. V. Pertsov, R. Salomonsz, W. Baxter, and J. Jalife, "Stationary and drifting spiral waves of excitation in isolated cardiac muscle," Nature **355**, 349–351 (1992).
[11] M. G. Clerc, M. A. Ferré, S. Coulibaly, R. G. Rojas, and M. Tlidi, "Chimera-like states in an array of coupled-waveguide resonators," Opt. Lett. **42**, 2906–2909 (2017).
[12] A. U. Nielsen, Y. Xu, C. Todd, M. Ferré, M. G. Clerc, S. Coen, S. G. Murdoch, and M. Erkintalo, "Nonlinear localization of dissipative modulation instability," Phys. Rev. Lett. **127**, 123901 (2021).
[13] E. A. Viktorov, T. Habruseva, S. P. Hegarty, G. Huyet, and B. Kelleher, "Coherence and incoherence in an optical comb," Phys. Rev. Lett. **112**, 224101 (2014).
[14] L. Yuan, Q. Lin, M. Xiao, and S. Fan, "Synthetic dimension in photonics," Optica **5**, 1396–1405 (2018).
[15] Y. Kuramoto and D. Battogtokh, "Coexistence of coherence and incoherence in nonlocally coupled phase oscillators," Nonlinear Phenom. Complex Syst. **5**, 380–385 (2002).
[16] R. Sarfati and O. Peleg, "Chimera states among synchronous fireflies," Sci. Adv. **8**, 6690 (2022).
[17] M. Sadilek and S. Thurner, "Physiologically motivated multiplex Kuramoto model describes phase diagram of cortical activity," Sci. Rep. **5**, 10015 (2015).
[18] B. Eckhardt, E. Ott, S. H. Strogatz, D. M. Abrams, and A. McRobie, "Modeling walker synchronization on the millennium bridge," Phys. Rev. E **75**, 021110 (2007).
[19] S. Nkomo, M. R. Tinsley, and K. Showalter, "Chimera states in populations of nonlocally coupled chemical oscillators," Phys. Rev. Lett. **110**, 244102 (2013).
[20] M. Piccardo, D. Kazakov, N. A. Rubin, P. Chevalier, Y. Wang, F. Xie, K. Lascola, A. Belyanin, and F. Capasso, "Time-dependent population inversion gratings in laser frequency combs," Optica **5**, 475–478 (2018).
[21] J. Hillbrand, D. Auth, M. Piccardo, N. Opačak, E. Gornik, G. Strasser, F. Capasso, S. Breuer, and B. Schwarz, "In-phase and anti-phase synchronization in a laser frequency comb," Phys. Rev. Lett. **124**, 023901 (2020).
[22] R. Rosales, S. G. Murdoch, R. T. Watts, K. Merghem, A. Martinez, F. Lelarge, A. Accard, L. P. Barry, and A. Ramdane, "High performance mode locking characteristics of single section quantum dash lasers," Opt. Express **20**, 8649–8657 (2012).
[23] M. Ossiander, D. Auth, J. Hillbrand, Q. Gaimard, D. Kazakov, M. Piccardo, A. Ramdane, F. Capasso, and S. Breuer, "Electrically injection-locked quantum dash frequency-modulated comb," in IEEE Conference on Lasers and Electro-Optics (CLEO), 2021.
[24] C. Kriso, A. Barua, O. Mohiuddin, C. Möller, A. Ruiz-Perez, W. Stolz, M. Koch, and A. Rahimi-Iman, "Signatures of a frequency-modulated comb in a VECSEL," Optica **8**, 458–463 (2021).

[25]L. A. Sterczewski, C. Frez, S. Forouhar, D. Burghoff, and M. Bagheri, "Frequency-modulated diode laser frequency combs at 2 μm wavelength," APL Photonics **5**, 076111 (2020).
[26]B. Schwarz, J. Hillbrand, M. Beiser, A. M. Andrews, G. Strasser, H. Detz, A. Schade, R. Weih, and S. Höfling, "Monolithic frequency comb platform based on interband cascade lasers and detectors," Optica **6**, 890–895 (2019).
[27]M. Singleton, P. Jouy, M. Beck, and J. Faist, "Evidence of linear chirp in mid-infrared quantum cascade lasers," Optica **5**, 948–953 (2018).
[28]J. Hillbrand, A. M. Andrews, H. Detz, G. Strasser, and B. Schwarz, "Coherent injection locking of quantum cascade laser frequency combs," Nat. Photonics **13**, 101–104 (2018).
[29]P. Täschler, A. Forrer, M. Bertrand, F. Kapsalidis, M. Beck, and J.Faist, "Asynchronous upconversion sampling of frequency modulated combs," Laser Photonics Rev. **17**, 220063 (2023).
[30]M. Piccardo, D. Kazakov, B. Schwarz, P. Chevalier, A. Amirzhan, J. Hillbrand, S. Z. Almutairi, Y. Wang, F. Xie, K. Lascola, S. Becker, L. Hildebrandt, R. Weih, A. Belyanin, and F. Capasso, "Light and microwaves in laser frequency combs: An interplay of spatiotemporal phenomena," IEEE J. Sel. Top. Quantum Electron. **25**, 9200112 (2019).
[31]A. Hugi, G. Villares, S. Blaser, H. C. Liu, and J.Faist, "Mid-infrared frequency comb based on a quantum cascade laser," Nature **492**, 229–233 (2012).
[32]D. Kazakov, M. Piccardo, Y. Wang, P. Chevalier, T. S. Mansuripur, F. Xie, C. Zah, K. Lascola, A. Belyanin, and F. Capasso, "Self-starting harmonic frequency comb generation in a quantum cascade laser," Nat. Photonics **11**, 789–792 (2017).
[33]M. Piccardo, P. Chevalier, B. Schwarz, D. Kazakov, Y. Wang, A. Belyanin, and F. Capasso, "Frequency-modulated combs obey a variational principle," Phys. Rev. Lett. **122**, 253901 (2019).
[34]N. Opačak and B. Schwarz, "Theory of frequency-modulated combs in lasers with spatial hole burning, dispersion, and Kerr nonlinearity," Phys. Rev. Lett. **123**, 243902 (2019).
[35]B. Schwarz, C. A. Wang, L. Missaggia, T. S. Mansuripur, P. Chevalier, M. K. Connors, D. McNulty, J. Cederberg, G. Strasser, and F. Capasso, "Watt-level continuous-wave emission from a bifunctional quantum cascade laser/detector," ACS Photonics **4**, 1225–1231 (2017).
[36]J. Hillbrand, N. Opačak, M. Piccardo, H. Schneider, G. Strasser, F. Capasso, and B. Schwarz, "Mode-locked short pulses from an 8 μm wavelength semiconductor laser," Nat. Commun. **11**, 5788 (2020).
[37]M. Piccardo, M. de Oliveira, A. Toma, V. Aglieri, A. Forbes, and A. Ambrosio, "Vortex laser arrays with topological charge control and self-healing of defects," Nat. Photonics **16**, 359–365 (2022).
[38]B. Chomet, T. Gabbrielli, D. Gacemi, F. Cappelli, L. Consolino, P. De Natale, F. Kapsalidis, A. Vasanelli, Y. Todorov, J. Faist, and C. Sirtori, "Anti-correlation phenomena in quantum cascade laser frequency combs," APL Photonics **8**, 106106 (2023).
[39]N. Opačak, B. Schneider, J.Faist, and B. Schwarz, "Impact of higher-order dispersion on frequency-modulated combs," arXiv:2310.09915 (2023).
[40]M. Piccardo, B. Schwarz, D. Kazakov, M. Beiser, N. Opačak, Y. Wang, S. Jha, J. Hillbrand, M. Tamagnone, W. T. Chen, A. Y. Zhu, L. L. Columbo, A. Belyanin, and F. Capasso, "Frequency combs induced by phase turbulence," Nature **582**, 360–364 (2020).
[41]B. Meng, M. Singleton, M. Shahmohammadi, F. Kapsalidis, R. Wang, M. Beck, and J. Faist, "Mid-infrared frequency comb from a ring quantum cascade laser," Optica **7**, 162–167 (2020).
[42]B. Meng, M. Singleton, J. Hillbrand, M. Franckié, M. Beck, and J.Faist, "Dissipative Kerr solitons in semiconductor ring lasers," Nat. Photonics **16**, 142–147 (2021).
[43]D. Kazakov, N. Opačak, M. Beiser, A. Belyanin, B. Schwarz, M. Piccardo, and F. Capasso, "Defect-engineered ring laser harmonic frequency combs," Optica **8**, 1277–1280 (2021).
[44]D. Kazakov, T.P. Letsou, M. Beiser, Y. Zhi, N. Opačak, M. Piccardo, B. Schwarz, and F. Capasso, "Active mid-infrared ring resonators," Nat. Commun. **15**(1), 607 (2024).